

Adam P. Hitchcock<sup>a,\*</sup>

# Influence of Local Environment on Inner Shell Excitation Spectra, Studied by Electron and X-ray Spectroscopy and Spectromicroscopy

<https://doi.org/10.1515/zpch-2017-1061>

Received October 20, 2017; accepted October 28, 2017

**Abstract:** Inner shell excitation spectroscopy is a local probe of the unoccupied electronic structure in the immediate vicinity of the core excited atom. As such, one might expect the inner shell spectrum of a given unit (a molecular fragment or a repeat unit of a solid) to be largely independent of where that unit is located. This is often an implicit assumption in spectral analysis and analytical applications. However, there are situations where inner shell excitation spectra exhibit significant sensitivity to their local environment. Here I categorize the ways in which inner shell spectra are affected by their local environment, and give examples from a career dedicated to developing a better understanding of inner shell excitation spectroscopy, its experimental techniques, and applications.

**Keywords:** electron energy loss; inner shell excitation spectroscopy; STXM; X-ray absorption.

## Highlights

- inner shell electrons are well shielded but still sense their local environment
- inner shell excitations are localized and often transferable among environments
- categorization of environment effects on inner-shell spectra of molecules, clusters, liquids, solids and heterogeneous materials
- examples from: water, peroxide, N<sub>2</sub>, amino acids, peptides, proteins, biphenyl, carboxylic acids.

---

<sup>a</sup>Issue in honor of Professor Eckart Rühl

\*Corresponding author: Adam P. Hitchcock, Department of Chemistry and Chemical Biology, McMaster University, Hamilton, ON L8S 4M1, Canada, Phone: +1 905 525-9140, e-mail: aph@mcmaster.ca

# 1 Introduction

In some cases, inner shell excitation spectra of a species (functional group, molecule, or solid) are quite independent of the local environment, whereas in other cases there are subtle, and sometimes dramatic, changes in the inner shell spectrum as the local environment of that species is changed. This article, in honor of Professor Eckart Rühl with whom I have collaborated over much of our scientific careers, is an attempt to categorize, and rationalize the effects of local environment on inner shell excitation spectra. As an experimentalist, I will use examples and stress a rather heuristic approach, but where appropriate, point to computational results addressing this subject.

Prior to the 1970s there was only a handful of papers reporting inner shell excitation, in large part due to the lack of suitable instrumentation. Through the pioneering work of Chris Brion, and his students (including me) the inner shell electron energy loss spectra (ISEELS) of many small molecules were recorded and interpreted [1, 2]. In the early 1980s high resolution soft X-ray synchrotron beamlines were developed, leading to the first near edge X-ray absorption fine structure spectroscopy (NEXAFS) studies of gases, solids and surfaces. In 1992 Jo Stöhr published his seminal monograph, NEXAFS Spectroscopy [3], which elegantly summarized experimental methods, theory, and applications of NEXAFS, primarily as applied to surface adsorbates. In the past few decades there has been a sustained growth of fundamental experimental and computational studies, development of electron energy loss and X-ray spectromicroscopies, and their application to a wide range of chemical, physical and materials problems. Recent reviews include: NEXAFS of large molecules (clusters, nanoparticles, biopolymers) measured typically by molecular beam and ionization methods [4]; NEXAFS of surfaces [5]; *in situ* NEXAFS of energy materials and process [6]. The influence of environment on inner shell excitation has been discussed from a theoretical perspective for a number of systems including: a variety of molecular gases [7] liquid water [8]; gas phase, cluster and liquid water and pyridine [9].

When considering the electronic structure of a system, emphasis is usually placed on the valence electrons since these are essential to bonding. Inner shell electrons are often ignored, being subsumed into the nucleus in some simple models. Spectroscopies such as UV-visible and fluorescence, based on valence electron excitation or ionization, are common. Relative to valence shell spectroscopy, inner shell spectroscopies (XPS, XAS, XES, EELS, etc) have some specific advantages – the signal can often be associated with a single atom or a functional unit, the experimental methods lend themselves to high resolution microscopies, many detection methods exist which allow optimization to different systems, etc.

Inner shell excitation involves conversion of energy supplied by an external probe (photon, electron, ion etc) to cause a transition between the initial, usually ground, state of the system to a core excited or ionized state. In most cases the core excited state can be described by a dominant electron configuration where one of the core levels of the system has one fewer electrons and the promoted electron is placed in a level (orbital or band) which was unoccupied in the initial state. The excited state is at high energy and generally decays very rapidly, having a lifetime of a few femtoseconds at most. While there are some observables indicating core holes can be exchanged among chemically equivalent sites (e.g. the two N atoms in N<sub>2</sub> [10]), descriptions based on localization of the core hole to a single atom are able to describe the vast majority of spectral features and phenomena. While the core hole is essentially localized on a single atom, the upper level can be either localized (as in many, but not all, core→valence excitations) or somewhat delocalized (as in core→Rydberg/exciton excitations). The presence of the core hole often significantly modifies the electronic structure [10]. The spectral details – energy, intensity, vibrational fine structure, lifetime, etc – will depend not just on properties of the core level, but also those of the ground-state-unoccupied valence (or Rydberg) upper level populated in the transition. Given that, why would one expect independence of local environment? Because core levels have a small spatial extent (20–50 pm) and thus they sample only a small portion of the unoccupied upper level, that which overlaps the core level. In many situations, that part of the final state electronic structure is often affected very little or not at all by changes that occur a bond length or farther away (>100 pm).

In discussions of inner shell excitation, core→valence excited states are those where the orbital/band of the upper level of the transition is constructed from atomic orbitals of the outermost principle quantum number ( $n$ ) of the atoms involved, e.g. the N 2p orbital in the case of N 1s→ $\pi^*$  transition of N<sub>2</sub>. Core→Rydberg/exciton excited states are those where the orbital/band of the upper level of the transition is constructed from atomic orbitals with  $n$  larger than the valence orbitals of the atoms involved, e.g. the N 3p orbital in the case of the N 1s→3p Rydberg transition of N<sub>2</sub>. Rydberg orbitals have a much larger size than valence orbitals, so they are expected to be more sensitive to changes in the local environment. Valence type core excited states are relatively compact and thus less likely to be influence by their environment. In the solid state, although a band picture is needed to describe the ground state, once a core excited state is created the electronic structure is perturbed around the localized core hole such that exciton descriptions – the solid state analogs of (core<sup>-1</sup>, valence) excitation – are appropriate. In addition, the high density of solids typically leads to quenching of Rydberg states. Finally extended X-ray absorption fine structure (EXAFS) is developed in molecules, and to an even larger extent in solids [11, 12].

The state-based quantum/spectroscopic interpretation [13] is of course the correct way to explain inner shell excitation spectra in detail. However, there are a number of heuristic approaches, such as bond length correlation [14], additivity [15] and fingerprinting [12, 16], which are commonly used, particularly in more practical applications of inner shell excitation. It is these types of situations to which this article is addressed. When considering inner shell excitation the influence of the local environment can be categorized in terms of the strength of the interaction, with effects occurring, roughly in order of decreasing magnitude of the changes created, by

- covalent or ionic bond formation
- electronic delocalization
- hydrogen bonding
- van der Waals and other weak interactions
- solvation

While these effects are not always independent of each other, they are a convenient framework in which to categorize the effects of environment on inner shell excitation spectra. This paper is organized as follows. After describing two of the instruments that both Professor Ruehl and I have used to acquire inner shell spectral data, examples of local effects on inner shell spectra are presented and discussed.

## 2 Experimental methods

### 2.1 ISEELS

Inner shell electrons can be excited and ionized with any probe which can provide the required excitation energy. The most common probes are X-ray photons and high kinetic energy monochromatic electrons. Except at many keV energies, X-ray absorption is governed by electric dipole selection rules [3]. The spectroscopic transitions that are created in an inelastic electron scattering event depend on the momentum transfer, which in turn depends on the incident electron energy and the scattering angle [2, 17]. At small momentum transfer, inner shell electron energy loss spectra (ISEELS) are dominated by electric dipole transitions and thus are directly comparable to near edge X-ray absorption spectra (NEXAFS), even quantitatively, if a small kinematic correction is applied [18]. All of the gas phase ISEELS examples discussed in this article were measured under electric dipole dominated conditions and thus are interpreted

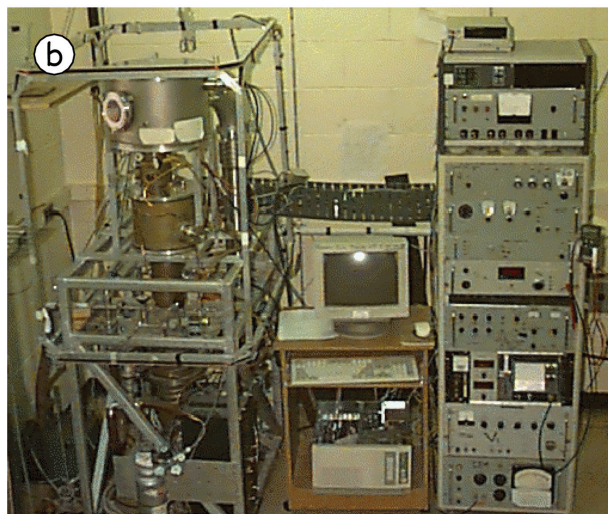
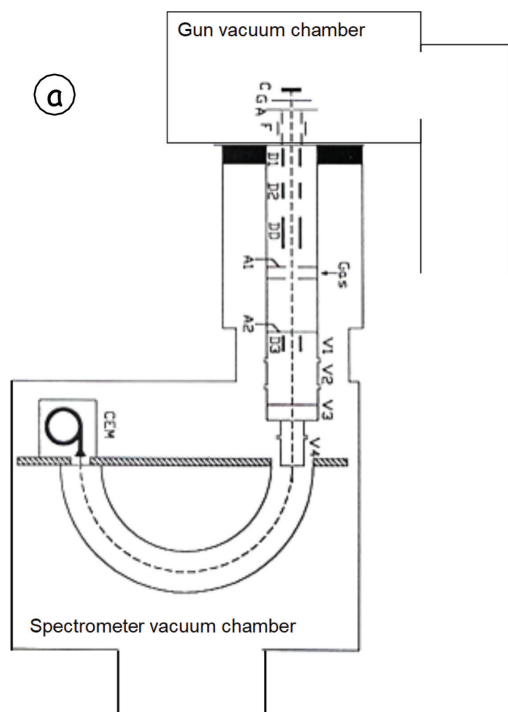


**Fig. 1:** (a) Dipole-regime inner shell electron energy loss spectrometer (ISEELS) for studies of the inner shell excitation spectra of gases. (b) Photograph of ISEELS instrument at McMaster University.

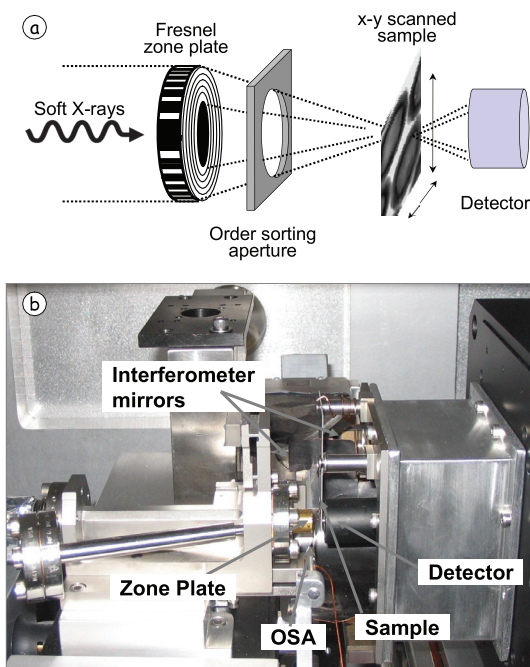


**Fig. 2:** (a) Schematic of a scanning transmission X-ray microscope (STXM). Monochromated soft X-rays from a beamline uniformly fill a Fresnel zone plate (ZP) which focuses 10–20% of the light to a point. An X-ray opaque central stop and the order sorting aperture (OSA) remove all but the first order focused light. The sample is positioned at the ZP focus and raster scanned orthogonal to the beam while detecting transmitted X-rays to generate an image. X-ray absorption spectra at any point, or at all positions in an area are measured by recording point intensities or full images at a sequence of X-ray energies. (b) photograph of the original polymer STXM at ALS BL 5.3.2.2 [23].

as being equivalent to X-ray absorption spectra. Figure 1a presents a schematic of the McMaster ISEELS spectrometer, while Figure 1b is a photo of the instrument. Since 1980 it has been used to record spectra of over 400 molecules. A database of these spectra, reported as raw data and also converted to quantitative optical oscillator strength scales, and a comprehensive bibliography of gas phase inner shell excitation are both available on my website [19]. As described in detail elsewhere [2], an electron beam generated from a B/W television electron gun is accelerated to  $(2.5 \text{ keV} + E_{\text{loss}} + E_{\text{pass}})$ , and directed into a gas cell with the target gas at  $\sim 1 \text{ mPa}$  ( $10^{-5}$  torr). Electrons inelastically scattered by  $\sim 2^\circ$  ( $0.03$  rad) are decelerated, and dispersed using a hemispherical analyzer. Those electrons with  $E_{\text{pass}}$  kinetic energy after deceleration pass through the exit aperture of the spectrometer and are detected in single electron counting mode. Spectra

are acquired using multi-pass signal averaging at a leisurely rate (~1–10 h/spectrum).

## 2.2 STXM

The X-ray absorption spectral data reported in this article were acquired using scanning transmission X-ray microscopy (STXM), a synchrotron based soft X-ray microscope technique, which is generally used to examine materials with high spatial resolution using spectromicroscopy approaches [20, 21]. Routine spatial resolution is 30 nm while state-of-the-art is 10 nm [22]. Figure 2a is a schematic of the microscope while Figure 2b is a photo of the focusing optics, sample region and part of the scanning mechanism of the original polymer STXM [23] at the Advanced Light Source (ALS) beamline 5.3.2.2 [24], which was the first of the modern interferometry controlled soft X-ray STXMs, which are now implemented in over 15 synchrotron facilities world wide. As described in detail elsewhere [21], X-rays from a bend magnet (ALS 5.3.2.2) or undulator source (ALS 11.0.2, CLS 10ID1 [25]) are monochromated and used to fully illuminate a Fresnel zone plate (ZP). The first order diffracted light is isolated using a combination of the ZP central stop and the order sorting aperture (OSA). The sample is placed at the focal point and (x, y) raster scanned while detecting transmitted X-rays in single photon counting mode. The transmission images are converted to optical density (OD) using the incident flux signal through a hole or non-sample support region. Spectra can be acquired in point or line modes, but most typically are acquired in image sequence mode, also called stacks [26]. For heterogeneous samples such as N<sub>2</sub> trapped at high pressure in a carbon nanotube discussed below, spectral/spatial fitting techniques available in aXis2000 [27] are used to convert stacks from transmission to optical density, and then to quantitative component maps, which can be combined into color coded composites to display spatial correlations of components.

## 2.3 Samples

In most cases the results presented in this article were previously published, and the reader is referred to those articles for details of samples and experimental conditions. In the case of the N<sub>2</sub> in a multi-walled carbon nanotube, the sample was prepared by ultrasonic spray pyrolysis [28], and placed on a 3 mm TEM grid coated with lacy carbon.

## 3 Results and discussion

### 3.1 Atomic, molecular, cluster comparative studies

Naively, if inner shell excitation was truly localized on a single atom and did not involve details of how that atom was linked to others, then atoms in ensembles

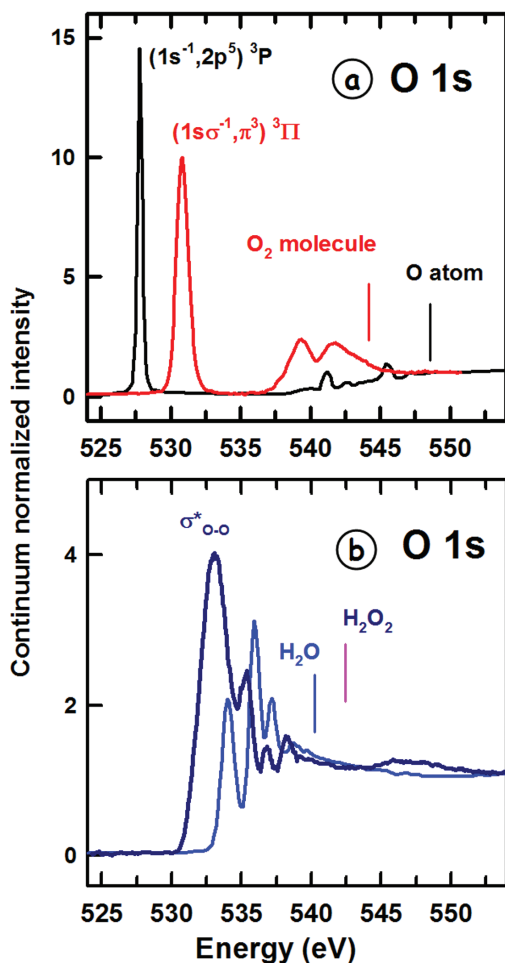


**Fig. 3:** (a) Comparison of the O 1s X-ray absorption spectrum of the O atom (digitized from [31]) to the O 1s ISEELS spectrum of the O<sub>2</sub> molecule [32]. (b) Comparison of the O 1s ISEELS spectra of gaseous water [33] and gaseous hydrogen peroxide [33, 34]. The vertical lines indicate the ionization limits as measured by X-ray photoelectron spectroscopy. For both figures, the intensity has been scaled so the intensity difference from 525 eV to 560 eV is 1.

such as clusters, liquids, solids or even compounds would be the same as the spectra of isolated atoms. In fact, for the rare gas atoms, this is not that bad an approximation, in that the inner shell spectra of solid and clusters of rare gas atoms such as Ar are similar to those of the atom, with mostly small spectral shifts related to polarization [29, 30], and development of extended fine structure (EXAFS) in the solid and with increasing cluster size. However, that situation is restricted to the rare gases. When all other atoms in the periodic table are combined, either covalent or ionic bonds are formed which have a marked effect on the inner shell spectrum. Figure 3a compares the O 1s spectra of the O atom [31] with that of O<sub>2</sub> [32]. The strong, sharp O (gs)→(O1s<sup>-1</sup>, 2p<sup>3</sup>) (<sup>3</sup>P) valence transition at 528 eV is transformed to a broad, strong O<sub>2</sub> (gs)→(O 1s<sup>-1</sup>, π<sup>\*3</sup>) <sup>3</sup>Π valence transition at 530.8 eV. Both atomic and molecular oxygen exhibit Rydberg transitions, although those in O<sub>2</sub> are superimposed on broad O<sub>2</sub> (gs)→(O 1s<sup>-1</sup>, π<sup>\*3</sup>) <sup>3</sup>Σ transitions at 539 and 542 eV [35, 36]. Thus the O–O bond formation makes a dramatic change to the O 1s spectrum of the O atom, with conversion of the atomic 1s→2p excitation into strong 1s→π<sup>\*</sup> and 1s→σ<sup>\*</sup> transitions. This trend is expected in most atom→molecule conversions since the formation of bonds from the overlap of orbitals on two atoms creates not only the occupied bonding levels which stabilize the molecule, but also partner unoccupied orbitals into which a core electron can be excited.

The evolution from spectra dominated by Rydberg transitions to ones dominated by valence transitions with formation of covalent bonds is well illustrated in Figure 3b which compares the O 1s ISEELS spectra of water (H<sub>2</sub>O) with that of hydrogen peroxide (H<sub>2</sub>O<sub>2</sub>) [33]. The spectrum of water is dominated by Rydberg states (although the lowest one has significant valence character). When a second O atom is inserted into one of the H–O bonds the newly created O–O bond leads to a broad 1s→σ<sup>\*</sup><sub>O–O</sub> transition at 533 eV and partial quenching of the Rydberg states.

A situation where one might expect relatively small impact of local environment on inner shell excitation spectra is that of weakly interacting molecular clusters, where the localized unoccupied π<sup>\*</sup> and σ<sup>\*</sup> levels associated with strong intramolecular covalent bonding are well shielded from the environment, whereas the more spatially extended Rydberg states are likely to be more susceptible to modification by interacting with neighbors. Rühl and collaborators have studied the inner shell excitation and photofragmentation of clusters of atoms and molecules extensively [37]. A nice example of the different effects on valence versus Rydberg states of a cluster environment is (N<sub>2</sub>)<sub>n</sub> (n ~ 150). Figure 4a,b presents results of a high energy resolution study of the N 1s π<sup>\*</sup> transition of (N<sub>2</sub>)<sub>n</sub> compared to that of gaseous molecular N<sub>2</sub> [38]. With exceptional care, a 6 ± 1 meV red shift in the energy of this transition was identified, and attributed to a dynamic polarization effect related to core hole localization. In contrast, the N 1s→Rydberg states in molecular N<sub>2</sub> are transformed to N 1s→exciton states, which

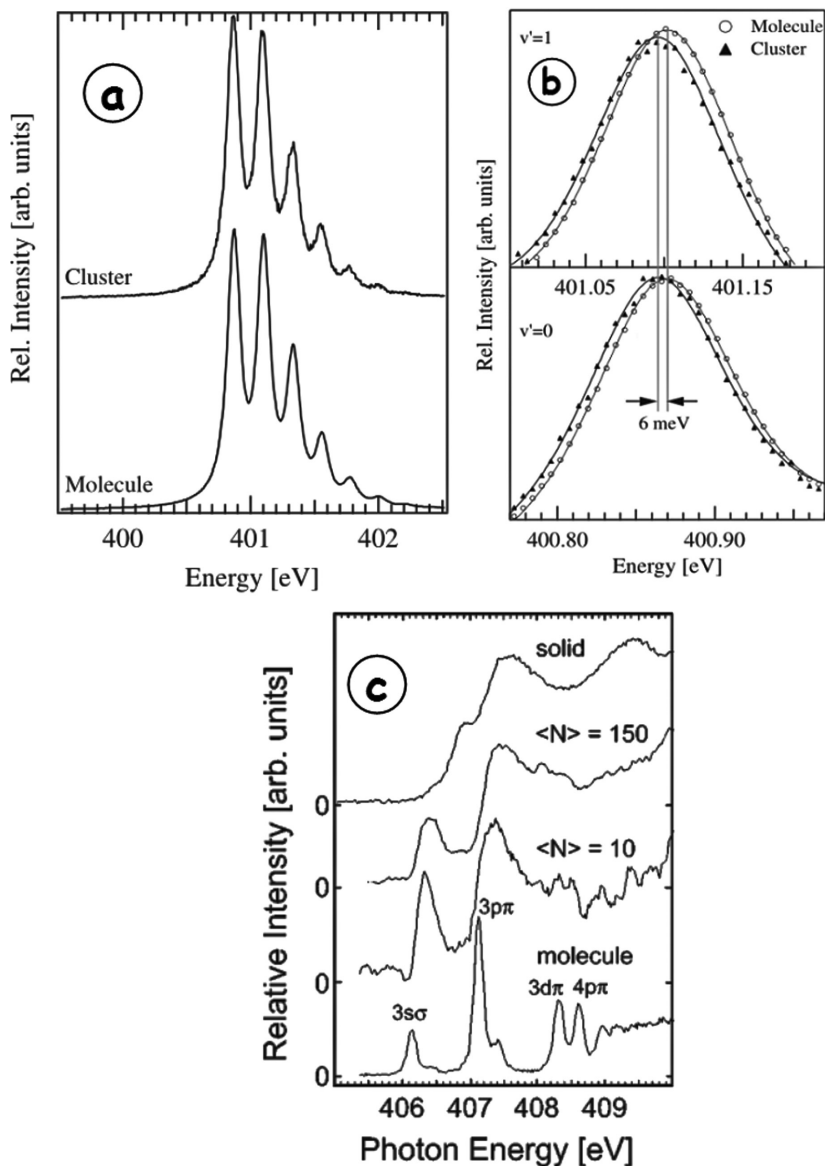


**Fig. 4:** (a)  $N\ 1s \rightarrow \pi^*$  region of the high resolution X-ray absorption spectrum, detected in total ion yield (TIY) mode, of  $N_2$  as a molecule, compared to the  $(N_2)_n^{2+}$  partial ion yield spectrum of a  $(N_2)_n$  cluster beam, with  $\langle n \rangle \sim 150$ . (b)  $v=0$  and  $v=1$  peaks of the  $1s \rightarrow 1\pi_g$  transition of molecular  $N_2$  (circles) and clustered  $(N_2)_n$  at  $\langle n \rangle \sim 150$  (triangles). The solid lines are fits to Voigt profiles [38]. (c) Comparison of the  $N\ 1s \rightarrow$  Rydberg region of  $N_2$  gas, to the  $N\ 1s \rightarrow$  exciton region of  $(N_2)_n$ ,  $\langle n \rangle = 10, 150$ , and solid  $N_2$ . There is a large blue shift and extensive line broadening between (cluster – gas) and (solid – gas) [39] (reproduced with permission).

are blue shifted by  $\sim 200$  meV in large clusters, and further shifted and broadened in the N 1s spectrum of solid  $N_2$  (see Figure 4c) [39].

Recently several groups have reported the inner shell spectra of  $N_2$  at high pressures trapped in multi-walled carbon nanotubes (MWCNT) [40, 41]. Figure 5a presents the N 1s spectrum of  $N_2$  in a MWCNT at a pressure of  $60 \pm 10$  atm, estimated from the optical density and diameter of the MWCNT. This spectrum and the unstructured spectrum of the tube wall were used to fit a N 1s stack to generate component maps of the MWCNT and the trapped  $N_2$  (Figure 5b). The data was recorded using the CLS ambient STXM, operated with a spatial resolution of 30 nm and an energy resolution of  $\sim 100$  meV. The spectrum of  $N_2$  gas recorded in the same system, using slightly higher energy resolution conditions, is also plotted in Figure 4c. In the context of this article several important changes are noted. As also reported by Zhou et al. [40], who used the same STXM, the vibrational fine structure of the N  $1s \rightarrow \pi^*$  transition is considerably blurred at high pressures, in contrast to the situation in clustered  $N_2$  (Figure 4a,b). The Rydberg features of the isolated gas are replaced by a broad, weakly structured band, in agreement with the exciton region of solid  $N_2$  (Figure 4c). An additional feature at  $\sim 404$  eV appears, probably due to interaction of the  $N_2$  with the carbon nanotube. There is a second N-containing component giving rise to the broad peak at 399.5 eV, which was attributed by Zhou et al. [40] to N substitution in the CNT walls, which had previously been identified by X-ray photoelectron and Raman spectroscopy [28].

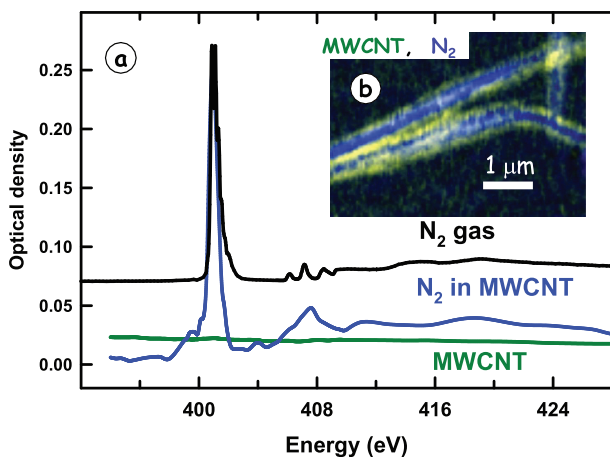


**Fig. 5:** (a) N 1s X-ray absorption spectrum of  $N_2$  (gas) and  $N_2$  trapped at high pressure in a multi-walled carbon nanotube (MWCNT), both recorded using STXM. The response of the MWCNT in the N 1s region is also plotted. (b) Color coded composite of the component maps of MWCNT and  $N_2$  (g), derived from fits to a N 1s stack (images at 68 energies from 394–430 eV) measured using the CLS ambient STXM (CLS, May 2017).

Several other examples where there are quite small changes in inner shell spectra with cluster or solid formation are benzene, where there is a  $-55$  meV red shift from gas to solid in the  $\nu=(000)$  line of the  $C\ 1s \rightarrow \pi^*$  transition, and the vibrational fine structure is remarkably identical [42]; and  $SF_6$ , where the strong  $S\ 2p \rightarrow t_{2g}$  continuum resonance transition is red shifted by  $-35$  meV while the  $S\ 2p \rightarrow e_g$  resonance is red shifted by  $105$  meV [43] between the gas and  $(SF_6)_n$ ,  $n > 40$  cluster. In the latter case, the weak  $S\ 2p \rightarrow$  Rydberg transitions were quenched in the solid state. Although not a cluster, carbonic acid ( $H_2CO_3$ ) – a short lived ( $\tau \sim 26$  ms) transient association of  $H_2O$  and  $CO_2$  – has been studied by NEXAFS using rapid mixing and liquid jets [44]. Through careful experimental measurements combined with high level quantum chemical calculations, the  $C\ 1s \rightarrow \pi^*_{C=O}$  signal was identified at  $290.45$  eV, overlapping those of  $CO_2$  (aq) ( $290.74$  eV) and  $HCO_3^-$  (aq) ( $290.30$  eV) with an intermediate intensity. Thus, in this case, changing the bond order from 2 to  $\sim 1.75$  then  $1.5$  causes an extremely small change in the transition energy. This is an interesting case, not just because of the tour de force measurement of a chemical species that many believed did not exist. It turns out that the energy of  $C\ 1s \rightarrow \pi^*_{C=O}$  transition is one of the most sensitive to local environment, with a span of energy from  $286$  to  $292$  eV [45]. The main factor determining the shift is changes in the type and the number of electronegative atoms bonded directly to the carbonyl carbon which is small in the case of the carbonic acid, bicarbonate case.

## 3.2 Additivity

Inner shell spectra are often interpreted as the sum of the spectra of molecular fragments, with in some cases, correction for effects of the removed and added bonds on the overall spectrum. For example, Figure 6a presents the  $C\ 1s$  ISEELS spectrum of phenylalanine compared to the appropriately intensity-weighted sum of the  $C\ 1s$  ISEELS of alanine and benzene, along with the  $C\ 1s$  spectra of those components [15]. One sees a remarkably good agreement of the sum with that of phenylalanine with each spectral feature observed, with similar intensity. The largest difference is in the width of the  $C\ 1s \rightarrow \pi^*$  transition, with that of phenylalanine appreciably broader than that of benzene, due to small chemical shifts in the  $C\ 1s$  (ring) core level energies associated with inductive effects of the alanine substituent. This approach has been used successfully to interpret the inner-shell spectra of many molecules and polymers. In the phenylalanine case the  $C-H$  bonds removed and the  $C-C$  bond formed have little influence on the spectrum.

In other cases, new bond formation between otherwise characteristic units can have a significant effect. A nice example is the peptide shift associated with

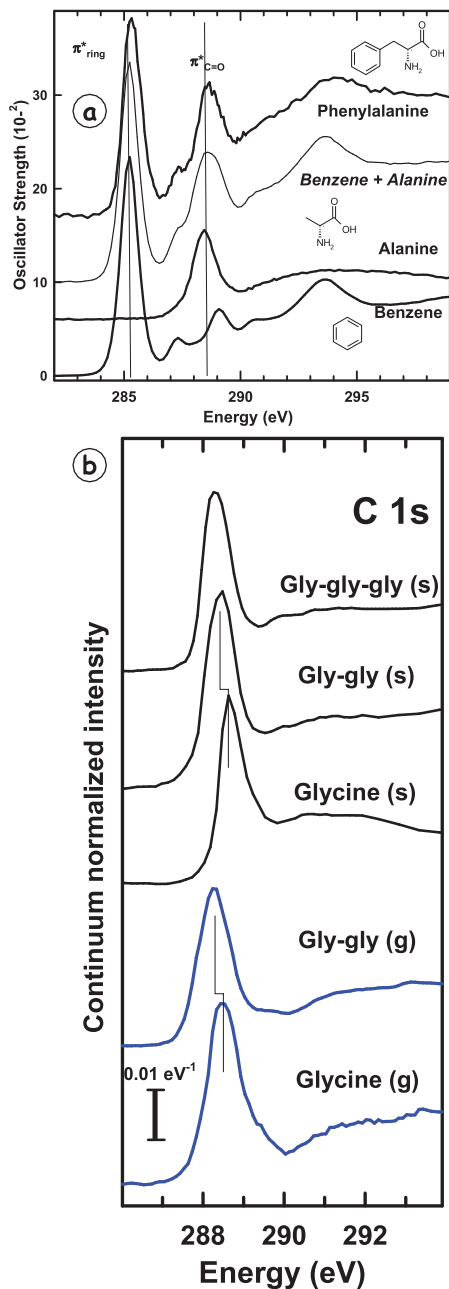
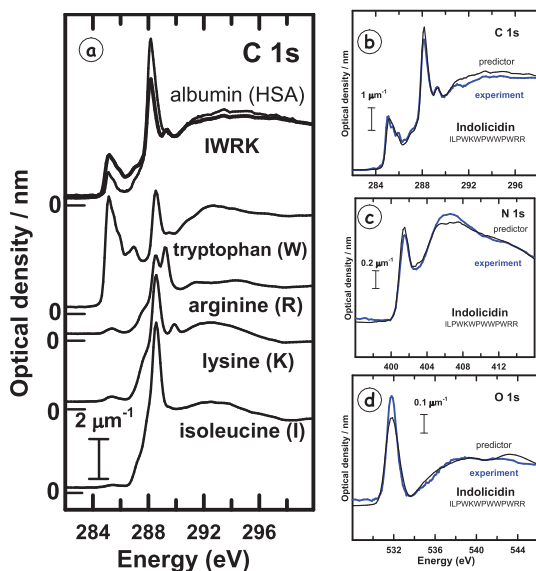


Fig. 6: (a) C 1s ISEELS spectrum of phenylalanine compared to those of benzene and alanine, and their sum [15]. (b) C 1s ISEELS spectra of gas phase glycine (gly) and diglycine, compared with XAS spectra of solid Gly, Gly-gly and Gly-gly-gly, recorded with STXM [46] (ALS 5.3.2.2, 2002).

converting a carboxylic acid and an amine group into a peptide bond. The effect is illustrated in Figure 6b, which compares the C 1s ISEELS spectra of gaseous glycine and the glycl-glycine dimer, as well as the NEXAFS spectra (recorded in STXM) of solid glycine, glycl-glycine and the Gly-gly-gly trimer [15, 46]. When the peptide bond is formed, the environment of the carbonyl carbon changes from one surrounded by two oxygens and one carbon to one oxygen, one nitrogen and one carbon. In consequence the C 1s(C=O) core level is shifted to lower binding energy, which shifts the C 1s(C=O)→ $\pi^*$  transition lower by 0.3 eV from 288.5 eV to 288.2 eV. The O 1s spectra of carbonyl oxygen in amino acids is also changed in peptides and proteins by a  $\sim$ 0.3 eV shift of the O 1s→ $\pi^*$  transition [15, 46]. An even more dramatic change occurs in the N 1s spectrum because the N environment of the amine terminal of isolated amino acids is saturated, whereas formation of the peptide bond introduces a partial double bond character due to delocalization of the  $\pi^*$  orbital over all three atoms of the peptide (amide) group [15, 46]. In fact the N 1s spectra of amino acids, peptides and proteins are remarkably sensitive to environmental changes, with significant changes in shape and appearance/disappearance of the N 1s (peptide)→ $\pi^*$ <sub>peptide</sub> peak at 402.1 eV with protonation or deprotonation and thus modification of a planar to a non-planar geometry [47, 48].

Because the changes in the  $\pi^*$ <sub>C=O</sub> peaks upon formation of the peptide bond are independent of the amino acids involved, it is possible to predict with quite remarkable accuracy the C 1s, N 1s and O 1s spectra of any amino acid sequence, and thus predict the spectra of peptides and proteins from their amino acid composition and the inner shell spectra of the individual amino acids [49]. The latter were recorded with very high quality and accuracy by Zubavichus et al. [50]. This capability is demonstrated in Figure 7a, which compares the C 1s, N 1s and O 1s spectra of the individual component amino acids to that of a small peptide, isoleucine-tryptophan-arginine-lysine (I-W-R-K, where I is Isoleucine, W is tryptophan, R is arginine and K is lysine) predicted using the method outlined by Stewart-Ornstein et al. [49]. The peptide spectrum is in turn compared to that of human serum albumin, showing that, at least for some compositions, it is feasible to differentiate peptides from large proteins [49]. Figure 7b, c, d plots the C 1s, N 1s and O 1s spectra of Indolicidin, another peptide with amino acid sequence ILPWKWPWWPWR, with that predicted from the amino acid sequence. Again, there is a substantial difference between the C 1s spectrum of this peptide, and that of a typical, mid-sized or large protein, as exemplified by human serum albumin. In fact initial optimism about the ability of inner shell spectroscopy to be used as a tool to identify specific proteins [50] had to be tempered since the high amount of averaging over the spectra of amino acids, combined with a frequently similar amino acid composition, leads to very similar C 1s, N 1s and



**Fig. 7:** (a) C 1s X-ray absorption spectra of Isoleucine, Lysine, Arginine and Tryptophan, [50] and their peptide-corrected sum, compared to that of albumin [49]. (b–d) Comparison of experimental C 1s (b), N 1s (c) and O 1s (d) NEXAFS spectra of indolicidin (ILPWKWPWW-PWRR-NH<sub>2</sub>) recorded in STXM, with those generated from the additivity principle with the peptide shift correction [49] (ALS 5.3.2.2, 2006).

O 1s spectra of mid-sized and large proteins [49, 51]. Still many peptides ( $n < 20$ ) will have sufficiently distinct inner shell spectra that they can be identified and mapped using spectromicroscopy techniques as illustrated by the X-ray photoemission electron microscopy (X-PEEM) studies of competitive binding of cationic antimicrobial peptides and albumin to a phase segregated polymer blend [52]. Very detailed studies of the effect of pH and salt concentration on the N 1s spectra of triglycine to investigate possible sensitivity to  $\alpha$ -helix versus  $\beta$ -sheet local folding ternary structure have been reported [53]. Liu et al. [54] succeeded in solving the conformation of RNase tethered in an ordered structure at the air terminus of an alkythiol self assembled monolayer, by a detailed analysis of the polarization dependent C 1s, N 1s, and S 1s NEXAFS. Stevens et al. [55] have investigated proton transfer, hydrogen bonding and salt effects in mixtures of bipyridine and organic acids. They observed small chemical shifts in the energies of N 1s  $\rightarrow \pi^*$  transitions which they could correlate with N–H distance or extent of proton transfer in hydrogen bonding.

Another factor that affects inner shell excitation spectra is  $\pi$ - $\pi$  delocalization in cases where there are alternating double and single bonds. Figure 8a presents

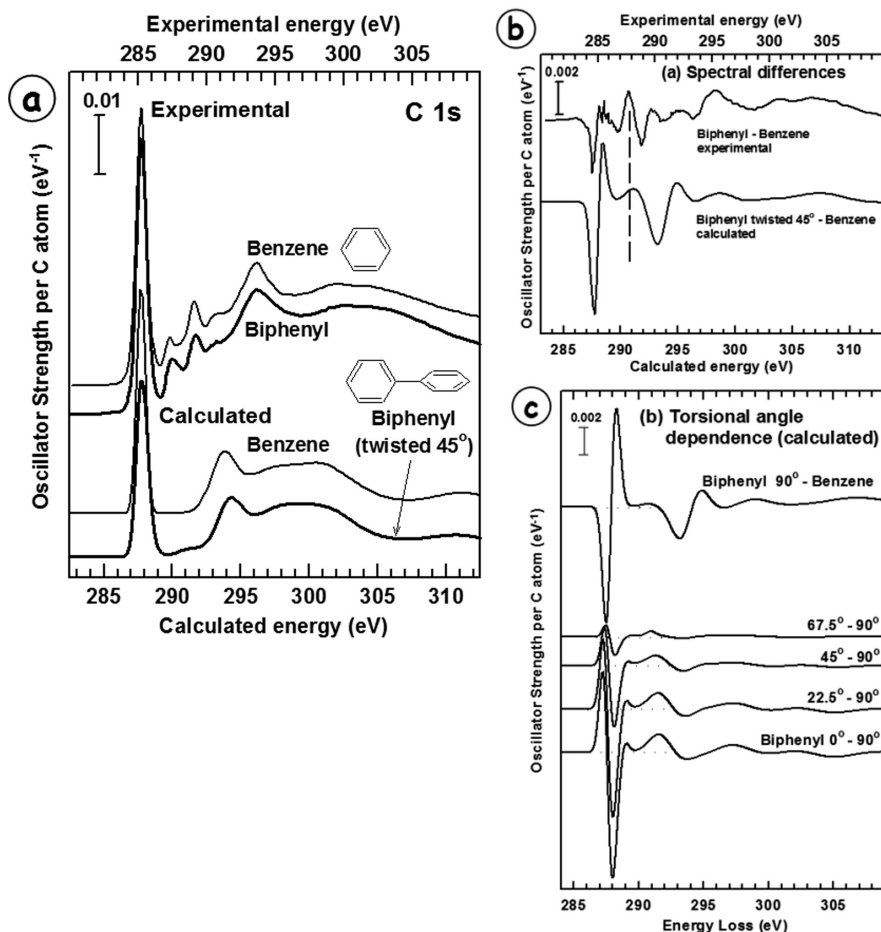


**Fig. 8:** (a) Experimental C 1s ISEELS spectrum of gas phase biphenyl compared to that of benzene and GSCF3 calculated spectra of benzene and 45°-twisted biphenyl. The calculated spectral energy scale is offset by  $-2.5$  eV to align with experiment. Vertical offsets are used for clarity [56]. (b) Difference of the experimental C 1s spectra of biphenyl and benzene, in comparison to the difference in the GSCF3 calculated C 1s spectra of 45°-twisted biphenyl and benzene [56]. (c) Difference of the calculated spectrum of 90°-twisted biphenyl with respect to those of other conformations, as well as the difference of the calculated spectra of 90°-twisted biphenyl and benzene [56].

ISEELS spectra of biphenyl in comparison to that of benzene and GSCF3 calculations of both species [56]. In the ground state the two phenyl rings of biphenyl are oriented at 45° with respect to each other so there is only partial delocalization across the C–C single bond connecting the two rings. Thus the

modification by ring-ring delocalization is smaller than it might be if the two rings were co-planar. The effects of delocalization versus replacement of two C–H bonds by one C–C bond were explored by examining the difference of biphenyl and twice the spectrum of benzene both experimentally (Figure 8b) and computationally (Figure 8c). In the computational study it is possible to turn off or enhance the delocalization by changing the ring-ring angle. Comparison of the computational and experimental spectral difference results identified a weak feature at 287.7 eV specifically arising from the ring-ring  $\pi^*$  delocalization [56]. In addition the centroid of the C  $1s \rightarrow 1\pi^*$  transition is shifted by  $\sim 0.1$  eV between benzene and biphenyl. Interestingly a NEXAFS study of face-on phenyl ring – phenyl ring interaction was recently reported in which the strength of the interaction was controlled by using either  $-\text{CH}_2-$  or  $-\text{CH}_2-\text{CH}_2-$  groups to link two benzene rings at the para positions [57]. In that situation a shift of 0.4 eV in the C  $1s \rightarrow 1\pi^*$  transition was observed.

### 3.3 Gas, surface, solid comparative studies

Since many molecular liquids or solids are held together by weak intermolecular forces (dipole-dipole, or induced dipole-induced dipole, van der Waal's forces) these may be cases where one would expect inner-shell excitation, particularly the stronger core  $\rightarrow$  valence excitations, to be relatively unaffected. In contrast one expects the spatially extended core  $\rightarrow$  Rydberg transitions to be either energy shifted or quenched. This is often true, so that, once effects of interaction among adjacent units are taken into account (e.g. peptides), the inner shell spectra of gas and solid phases of the same species are similar (see Figure 6). However, there are cases where there are geometric and electronic structure changes on condensation which strongly affect the inner shell spectra. Figure 9 compares the C  $1s$  and O  $1s$  ISEELS spectra of gaseous formic acid [58] with that of the NEXAFS spectra of formic acid adsorbed as a multilayer on a cold (120 K) Si(111) surface [59]. The C  $1s$  spectra (Figure 9a) of gas and solid are quite similar, aside from changes associated with linear dichroism in the case of the partly aligned molecules in the condensed multilayer, which, on average, have the plane of the formic acid molecule tilted  $35^\circ$  relative to the surface [59]. The C  $1s \rightarrow \pi^*$  transition occurs at the same energy, while the gas phase Rydberg features are broadened and blue shifted in the solid. However, the O  $1s$  spectrum of formic acid gas (Figure 9c) is dramatically different from that of condensed formic acid, and not just because of the linear dichroism. In fact the two sharp peaks at 532 eV and 535 eV in the gas phase are merged into a single broad peak at 533

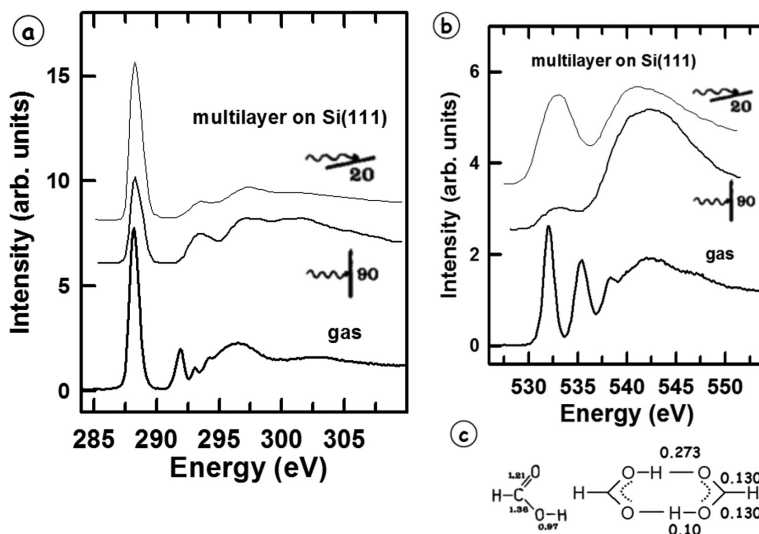


**Fig. 9:** (a) C 1s and (b) O 1s ISEELS spectrum of gaseous formic acid [58], compared to the C 1s and O 1s total electron yield polarization dependent NEXAFS spectra of a multilayer of formic acid deposited on a Si(111) substrate at 120 K [59]. The orientation of the incident X-rays and the surface is indicated. The spectral changes are consistent with the molecules having an average tilt of 35° relative to the surface [59]. (c) Structure and bond lengths of monomer and dimer formic acid [60].

eV in the solid. In the gas phase the isolated molecules have distinct C=O and C–O–H environments, leading to a shift of 3 eV between the O 1s(C=O)→ $\pi^*_{C=O}$  and O 1s(C–O)→ $\pi^*_{C-O}$  transitions. In contrast, in the solid state, there is dimer formation caused by H-bonding which means that the two oxygen atoms are identical chemical environments in the condensed phase (see structural sketches in Figure 9b). A single O 1s→ $\pi^*$  transition is also found in the NEXAFS spectra of other condensed carboxylic acids (propionic acid, acrylic acid [59]), while the O 1s spectrum of the same species in the gas phase shows two O 1s→ $\pi^*$  transitions [61]. The sensitivity of the O 1s excitation spectrum of carboxylic acids to hydrogen bonding is the largest effect of H-bonding of which I am aware. It is an indirect effect whereby the hydrogen bond formation induces other structural changes (in the case of carboxylic acids, equalizing the two O environments), which in turn give rise to a more dramatic spectral change than would be expected just from protonation. There are several other situations where hydrogen bonding effects on inner shell excitation spectra have been reported [62, 63]. Since hydrogen bonding and other directional intermolecular interactions play an important role in determining peptide and protein conformations, the sensitivity of inner shell excitation spectra to hydrogen bonding is of use in biochemical studies by inner shell excitation spectroscopies [54].

The final example I wish to highlight is the remarkable phase sensitivity of the O 1s spectrum of water. Figure 10 presents the O 1s spectra of gas [66], liquid [64, 67] and solid [65, 68] water on an absolute intensity scale (OD/nm at a density of  $1 \text{ g} \cdot \text{cm}^{-3}$ ). As noted in the discussion of Figure 3, the spectrum of water vapor is dominated by core  $\rightarrow$  Rydberg transitions, although the upper level of the lowest energy O 1s  $a_1 \rightarrow 4s a_1$  transition has significant antibonding O–H character, as indicated by extensive vibrational excitation to a repulsive potential surface leading to ultrafast dissociation [69, 70]. The sharp  $4s a_1$  peak in the gas is shifted and broadened into the 535 eV “pre-peak” in liquid and solid water. Higher energy Rydberg transitions in the gas are merged into a two peaked band structure from 537–545 eV. There are extensive experimental studies, theoretical calculations and associated discussion of the interpretation of the spectra of liquid and solid water, which can be found in a whole journal volume dedicated to the subject – J. Electron Spectrosc. Rel. Phenom. 177 (2010) – and subsequent literature citing those articles. Sahle et al. [71] have recently reported a study of the O 1s excitation spectrum of liquid water combining *ab initio* molecular dynamics to compute geometric structures, Bethe-Salpeter *ab initio* calculations of the inelastic X-ray scattering (IXS) spectra, and experimental IXS spectra [72]. The results reinforce the subtle but interpretable link between inner shell excitation spectra and changes in the local environment in water. It would appear that subtle aspects of the O 1s spectrum of liquid water are related to changes

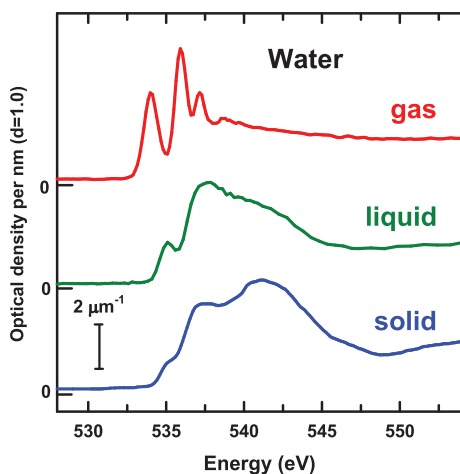


**Fig. 10:** Comparison of the O 1s spectra of water in the gas phase [33, 58], liquid [64] and solid (ice) [65] states. The intensities have been adjusted to be the optical density for 1 nm (OD1) assuming a density of  $1.0 \text{ g} \cdot \text{cm}^{-3}$  for all three phases.

in distributions of donor and acceptor hydrogen bonding, which in turn are affected by the presence of solutes such as salts, and biomacromolecules such as proteins. Thus the fine details of the O 1s spectrum of water are being used to indirectly probe the environment of solutes, and their affect on the dynamic structure of water.

## 4 Summary

Through examples I have outlined various ways in which inner shell excitation spectra can be influenced by changes in the local environment of the core excited atom, molecule, or repeat unit of a condensed phase. The use of a transferability assumption is justified in some cases, but not in others. Understanding the origins and types of effects of different environments on inner shell excitation will help guide spectral interpretation and identification of those situations where spectral modification by new bond formation or by intermolecular or condensed phase interactions are to be expected.

**Acknowledgements:** I wish to acknowledge the many and diverse scientific collaborations I have had with Professor Eckart Rühl – we have over 25 joint publications, dating from 1989 through to 2014. It has been an honor to work together with him and his group, and a real pleasure to have him as a lifelong friend. The funding needed to acquire the ISEELS and STXM results presented in this article has been provided by the Natural Sciences and Engineering Research Council of Canada (NSERC). STXM results have been recorded using several beamlines at the ALS (Lawrence Berkeley National Lab), funded by the Basic Energy Sciences division of the US Department of Energy, and with the ambient STXM on beamline 10ID1 at the Canadian Light Source (CLS, Saskatoon) which is funded by the Canada Foundation for Innovation, NSERC, the University of Saskatchewan, the Government of Saskatchewan, Western Economic Diversification Canada, the National Research Council Canada, and the Canadian Institutes of Health Research.

## References

1. A. P. Hitchcock, *Phys. Scripta* **T31** (1990) 159.
2. A. P. Hitchcock, *J. Electron Spectroscopy Rel. Phenom.* **112** (2000) 9.

3. J. Stöhr, NEXAFS spectroscopy, Springer, Berlin (1992).
4. A. R. Milosavljević, A. Giuliani, C. Nicolas, Chapter 8, in: X-ray and Neutron Techniques for Nanomaterials Characterization, C. S. S. R. Kumar (Ed.), Springer-Verlag, Berlin (2016).
5. M. B. Casu, T. Chassé, NEXAFS studies at surfaces, in: Handbook of Spectroscopy, 2<sup>nd</sup> ed. G. Gauglitz, D. S. Moore (Eds.), Wiley-VCH Verlag GmbH & Co. KGaA, Weinheim, Germany (2014).
6. X. Liu, W. Yang, Z. Liu, Adv. Mater **2** (2014) 7710.
7. T. Plashkevych, H. Privalov, H. Agren, V. Carravetta, K. Ruud, Chem. Phys **260** (2000) 11.
8. Ph. Wernet, D. Nordlund, U. Bergmann, M. Cavalleri, M. Odelius, H. Ogasawara, L. Å. Naslund, T. K. Hirsch, L. Ojamae, P. Glatzel, L. G. M. Pettersson, A. Nilsson, Science **304** (2004) 995.
9. M. Iannuzzi, J. Hutter, Phys. Chem. Chem. Phys. **9** (2007) 1599.
10. M. S. Schöffler, J. Titze, N. Petridis, T. Jahnke, K. Cole, L. P. Schmidt, A. Czasch, D. Akoury, O. Jagutzki, J. B. Williams, N. A. Cherepkov, S. K. Semenov, C. W. McCurdy, T. N. Rescigno, C. L. Cocke, T. Osipo, S. Lee, M. H. Prior, A. Belkacem, A. L. Landers, H. Schmidt-Böcking, T. Weber, R. Dörner, Science **320** (2008) 920.
11. L. Triguero, L. G. M. Pettersson, H. Agren, Phys. Rev. B **58** (1998) 8097.
12. M. Newville, Rev. Mineral. Geochem. **78** (2014) 33.
13. I. N. Levine, Quantum Mechanics, 7<sup>th</sup> ed. Pearson, NY (2013).
14. F. Sette, J. Stöhr, A. P. Hitchcock, J. Chem. Phys. **81** (1984) 4906.
15. G. Cooper, M. Gordon, D. Tulumello, C. C. Turci, K. Kaznatcheev, A. P. Hitchcock, J. Electron Spectroscopy Rel. Phenom. **137–140** (2004) 795.
16. J. R. Lawrence, G. D. W. Swerhone, G. G. Leppard, T. Araki, X. Zhang, M. M. West, A. P. Hitchcock, Appl. Environ. Microbiol. **69** (2003) 5543.
17. R. F. Egerton, Rep. Prog. Phys. **72** (2009) 016502.
18. R. McLaren, S. A. C. Clark, I. Ishii, A. P. Hitchcock, Phys. Rev. A **36** (1987) 1683.
19. Hitchcock. 2017. database: <http://unicorn.mcmaster.ca/corex/cedb-title.html>; bibliography: [http://unicorn.mcmaster.ca/xrm-biblio/xrm\\_bib.html](http://unicorn.mcmaster.ca/xrm-biblio/xrm_bib.html). Accessed 20 October 2017.
20. H. Ade, A. P. Hitchcock, Polymer **49** (2008) 643.
21. A. P. Hitchcock, Chapter 22, in: Volume II of the Handbook on Nanoscopy, G. Van Tendeloo, D. Van Dyck, S. J. Pennycook (Eds.), Wiley, New York (2012), p. 745.
22. W. Chao, P. Fischer, T. Tyliczszak, S. Rekawa, E. Anderson, P. Naulleau, Opt Express **20** (2012) 9777.
23. A. L. D. Kilcoyne, T. Tyliczszak, W. F. Steele, S. Fakra, P. Hitchcock, K. Franck, E. Anderson, B. Harteneck, E. G. Rightor, G. E. Mitchell, A. P. Hitchcock, L. Yang, T. Warwick, H. Ade, J. Synchrotron Radiat. **10** (2003) 125.
24. T. Warwick, H. Ade, A. L. D. Kilcoyne, M. Kritscher, T. Tyliczszak, S. Fakra, A. P. Hitchcock, P. Hitchcock, H. A. Padmore, J. Synchrotron Radiat. **9** (2002) 254.
25. K. V. Kaznatcheev, Ch. Karunakaran, U. D. Lanke, S. G. Urquhart, M. Obst, A.P. Hitchcock, Nucl. Inst. Meth. A **582** (2007) 96.
26. C. Jacobsen, S. Wirrick, G. Flynn, C. Zimba, J. Microscopy **197** (2000) 173.
27. A. P. Hitchcock, aXis2000 is written in Interactive Data Language (IDL). It is available free for non-commercial use from <http://unicorn.mcmaster.ca/aXis2000.html>. Accessed 20 October 2017.
28. J. Liu, Y. Zhang, M. I. Ionescu, R. Li, X. Sun, Appl. Surf. Sci. **257** (2011) 7837.
29. E. Rühl, C. Heinzl, A. P. Hitchcock, H. Baumgärtel, J. Chem. Phys. **98** (1993) 2653.
30. E. Rühl, C. Heinzl, A. P. Hitchcock, H. Schmeltz, C. Reynaud, H. Baumgärtel, W. Drube, R. Frahm, J. Chem. Phys. **98** (1993) 6820.

31. M. O. Krause, C. D. Caldwell, A. Menzel, S. Benzaud, J. Jimenez-Mier, *J. Electron Spectroscopy Rel. Phenom.* **79** (1996) 241.
32. A. P. Hitchcock, C. E. Brion, *J. Electron Spectroscopy Rel. Phenom.* **18** (1980) 1.
33. E. Rühl, A. P. Hitchcock, *Chem. Phys.* **154** (1991) 323.
34. K. L. Harding, S. Kalirai, R. Hayes, V. Ju, G. Cooper, A. P. Hitchcock, M. R. Thompson, *Chem. Phys.* **461** (2015) 117.
35. K. J. Randall, W. Eberhardt, J. Feldhaus, W. Erlebach, A. M. Bradshaw, Z. Xu, P. D. Johnson, Y. Ma, *Nucl. Inst. Meth. A* **319** (1992) 101.
36. A. Kivimaki, B. Kempgens, M. N. Piancastelli, M. Neeb, K. Maier, A. Rudel, U. Hergerhahn, A. M. Bradshaw, *J. Electron Spectroscopy Rel. Phenom.* **93** (1998) 81.
37. E. Rühl, *Int. J. Mass Spectrom.* **229** (2003) 117.
38. R. Flesch, A. A. Pavlychev, J. J. Neville, J. Blumberg, M. Kuhlmann, W. Tappe, F. Senf, O. Schwarzkopf, A. P. Hitchcock, E. Rühl, *Phys. Rev. Lett.* **86** (2001) 3767.
39. R. Flesch, N. Kosugi, I. Bradeanu, J. J. Neville, E. Rühl, *J. Chem. Phys.* **121** (2004) 8343.
40. J. Zhou, J. Wang, H. Liu, M. N. Banis, X. Sun, T. K. Sham, *J. Phys. Chem. Lett.* **1** (2010) 1709.
41. S. Stamboula, PhD thesis, McMaster University, Hamilton, Canada, 2018.
42. R. Flesch, E. Serdaroglu, F. Blobner, P. Feulner, X. O. Brykalova, A. A. Pavlychev, N. Kosugi, E. Rühl, *Phys. Chem. Chem. Phys.* **14** (2012) 9397.
43. R. Flesch, E. Seardarogu, X. O. Brykalova, E. I. Kan, E. S. Klyushina, Yu. S. Krivosenko, A. A. Pavlychev, E. Rühl, *J. Chem. Phys.* **138** (2013) 144302.
44. R. K. Lam, A. H. England, A. T. Sheardy, O. Shih, J. W. Smith, A. M. Rizzuto, D. Prendergast, R. J. Saykally, *Chem. Phys. Lett.* **614** (2014) 282.
45. S. G. Urquhart, H. Ade, *J. Phys. Chem. B* **106** (2002) 8531.
46. M. L. Gordon, G. Cooper, C. Morin, T. Araki, C. C. Turci, K. Kaznatcheev, A. P. Hitchcock, *J. Phys. Chem A* **107** (2003) 6144.
47. E Otero, S. G. Urquhart, *J. Phys. Chem A* **110** (2006) 12121.
48. Y. Zubavichus, A. Shaporenko, M. Grunze, M. Zharnikov, *J. Phys. Chem. B* **110** (2006) 3420.
49. J. Stewart-Ornstein, A. P. Hitchcock, D. Hernández-Cruz, P. Henklein, J. Overhage, K. Hilpert, J. Hale, R. E. W. Hancock, *J. Phys. Chem. B* **111** (2007) 7691.
50. Y. Zubavichus, A. Shaporenko, M. Grunze, M. Zharnikov, *J. Phys. Chem. A* **109** (2005) 6998.
51. Y. Zubavichus, A. Shaporenko, M. L. Grunze, M. Zharnikov, *J. Phys. Chem. B* **112** (2008) 4478.
52. B. O. Leung, A. P. Hitchcock, J. L. Brash, A. Scholl, A. Doran, P. Henklein, J. Overhage, K. Hilpert, J. D. Hale, R. E. W. Hancock, *Biointerphases* **3** (2008) F27.
53. C. P. Schwartz, J. S. Uejio, A. M. Duffin, A. H. England, D. N. Kelly, D. Prendergast, R. J. Saykally, *Proc. Nat. Acad. Sci.* **107** (2010) 14008.
54. X. Liu, C. H. Jang, F. Zheng, A. Jürgensen, J. D. Denlinger, K. A. Dickson, R. T. Raines, N. L. Abbott, F. J. Himpsel, *Langmuir* **22** (2006) 7719.
55. J. S. Stevens, L. K. Newton, C. Jaye, C. A. Murny, D. A. Fischer, S. L. M. Schroeder, *Cryst. Growth Des.* **15** (2015) 1776.
56. J. Wang, G. Cooper, D. Tulumello, A. P. Hitchcock, *J. Phys. Chem. A* **109** (2005) 10886.
57. S. D. Perera, S. G. Urquhart, *J. Phys. Chem A* **121** (2017) 4907.
58. I. Ishii, A. P. Hitchcock, *J. Chem. Phys.* **87** (1987) 830.
59. D. A. Outka, J. Stohr, R. J. Madix, H. H. Rotermund, B. Hermsmeier, J. Solomon, *Surf. Sci.* **185** (1987) 53.
60. R. J. Jakobsen, Y. Mieawa, J. W. Brasch, *Spectrochim. Acta A* **23** (1967) 2199.
61. I. Ishii, A. P. Hitchcock, *J. Electron Spectroscopy Rel. Phenom.* **46** (1988) 55.

62. A. Ganesan, F. Wang, *J. Chem. Phys.* **131** (2009) 044321.
63. G. Olivieri, A. Cossaro, E. Capria, L. Benevoli, M. Coreno, M. De Simone, K. C. Prince, G. Kladnik, D. Cvetko, B. Fraboni, A. Morgante, L. Floreano, A. Fraleoni-Morgera, *J. Phys. Chem. C* **119** (2015) 121.
64. C. D. Cappa, J. D. Smith, W. R. Wilson, R. J. Saykally, *J. Phys.: Condens. Matter* **20** (2008) 205105.
65. H. Bluhm, D. Frank Ogletree, C. S. Fadley, Z. Hussain, M. Salmeron, *J. Phys. C* **14** (2002) L221.
66. I. Ishii, R. McLaren, A. P. Hitchcock, M. B. Robin, *J. Chem. Phys.* **87** (1987) 4344.
67. K. R. Wilson, B. S. Rude, T. Catalano, R. D. Schaller, J. G. Tobin, D. T. Co, R. J. Saykally, *J. Phys. Chem. B* **105** (2001) 3346.
68. A. Nilsson, D. Nordlund, I. Waluyo, N. Huang, H. Ogasawara, S. Kaya, U. Bergmann, L.-Å. Näslund, H. Öström, Ph. Wernet, K. J. Andersson, T. Schiros, L. G. M. Pettersson, *J. Electron Spectroscopy Rel. Phenom.* **177** (2010) 99.
69. I. Hjelte, M. N. Piancastelli, R. Fink, Reinhold, O. Björneholm, M. Bässler, R. Feifel, A. Giertz, K. Wiesner, A. Ausmees, C. Miron, Catalin, H. Wang, S. Sorensen, S. Svensson, *Chem. Phys. Lett.* **334** (2001) 151.
70. B. Brena, D. Nordlund, M. Odelius, H. Ogasawara, A. Nilsson, L. G. M. Pettersson, *Phys. Rev. Lett.* **93** (2004) 148302.
71. C. J. Sahle, J. Niskanen, K. Gilmore, S. Jahn, *J. Electron Spectroscopy Rel. Phenom.* (2017) in press. doi: 10.1016/j.elspec.2017.09.003.
72. C. J. Sahle, C. Sternemann, S. Schmidt, S. Lehtola, S. Jahn, S. Simonelli, S. Huotari, M. Hakala, T. Pykkänen, A. Nyrow, K. Mende, M. Tolan, K. Hämäläinen, M. Wilke, *Proc. Nat. Acad. Sci.* **110** (2013) 6301.